Development of NEMESI: A Multiparameter Library Generator Prototype for Industrial VVER and PWR Applications Based on APOLLO3®

A. Brighenti,[a]* B. Vezzoni,[a] A. Hebert,[b] B. Calgaro,[a] E. Y. Garcia-Cervantes,[c] G. Huaccho Zavala,[d] L. Graziano,[a] P. Laurent,[e] L. Mercatali,[d] P. Mosca,[f] A. Previti,[a] S. Santandrea,[f] J. F. Vidal,[c] A. Willien,[e] and I. Zmijarevic[f]

[a]*Framatome, DTIPD Codes and Methods Department, Paris-la-Défense, France*
[b]*Polytechnique Montréal, Montréal, QC, Canada*
[c]*CEA Cadarache - SPRC/LEPH, Saint-Paul-Lez-Durance, France*
[d]*Karlsruhe Institute of Technology, Eggenstein-Leopoldshafen, Germany*
[e]*EDF Lab Paris-Saclay, Palaiseau, France*
[f]*Université Paris-Saclay, CEA Saclay – SERMA, Gif-sur-Yvette, France*

Abstract — *A nuclear reactor's design and safety assessment relies on a calculation platform consisting of a series of calculations performed using different simulation tools, each dedicated to modeling a specific phenomenon. The European Union H2020 CAMIVVER Work Package 4 aims to establish lattice neutronics calculation methodologies for VVER and pressurized water reactor fuel assemblies employing the new-generation deterministic multipurpose neutron transport code APOLLO3®, developed by the CEA (Commissariat à l'Energie Atomique et aux Energies Alternatives) with the support of EDF (Electricité de France) and Framatome.*

The present work aims to present NEMESI, an industrial prototype of a flexible lattice calculation tool developed as part of the CAMIVVER project, showing the applicability of APOLLO3 for industrial research and development and proposing dedicated VVER calculation schemes. Given the intense focus on the industrial issues of the entire CAMIVVER project, the elements constituting the rationale behind the development of such a computational platform are flexible modeling and analysis options, compliance with a series of specified requirements, implementation of innovative algorithms with improved precision, and a modern software and architectural base.

Keywords — *NEMESI, APOLLO3®, VVER/PWR, neutron transport, verification validation.*

I. INTRODUCTION

The work presented in this paper is integrated within the European Union (EU) H2020 CAMIVVER project,[1] which aims to investigate a new generation of innovative codes and methods oriented toward improving the comprehension of the physical phenomena occurring in the core under steady-state and transient conditions of western pressurized water reactor (PWR) and VVER reactor types, as presented in Refs. [2,3]. Specifically, Work Package 4 is devoted to setting up the framework for the development of an industrial calculation

*E-mail: alberto.brighenti@framatome.com

platform for lattice neutronics analysis and generating multiparameter data libraries for core calculations using APOLLO3®,[4] the new-generation deterministic code for lattice and core calculations developed by the Commissariat à l'Énergie Atomique et aux Énergies Alternatives (CEA) with the support of Framatome and Électricité de France (EDF).

For industrial applications, besides the need for the accuracy and precision of the solvers, a calculation platform should provide users with a feature that allows for flexibility in the choice of the modeling parameters and simulation options. The multiparameter library generator prototype described in this paper, called NEMESI, is the outcome of a more extensive work presented in Ref. [5], i.e., the identification and definition of users' needs for performing lattice calculations for the nuclear industry on different types of fuel assembly geometries (hexagonal and squared) and for Generation-II and Generation-III light water reactor (LWR) applications.

This paper presents the preliminary results obtained on selected western PWR and VVER assembly types using the reference computational scheme and the comparisons against reference Monte Carlo calculations. This paper also shows how the platform can be used to change different simulating parameters composing a calculation scheme, here the self-shielding grouping, and how this choice affects the results.

II. DEVELOPMENT OF NEMESI

Several deterministic or stochastic neutronics codes are currently available (see Ref. [6]). However, their level of technical complexity does not always meet the needs of their various users. It is therefore required to go beyond the concept of a neutronics code and think instead of a "neutronics platform" that should provide an interface suitable for all potential users.

As underlined in Ref. [5], research calculation codes often have a monolithic structure. Different from the library-based structure, in the monolithic structure the data belong to the code and not to the user. To make an example, a tool that parses an input file and runs until the end of the simulation is often monolithic, while on the other side, using a library-based tool the user can successively interact with the library and intervene during the execution. Any shared library follows this principle. Such conditions may make the software structure challenging to understand and maintain because the computational kernel (back end) creates and owns, as an internal state, all the data that can be modified during the execution only by internal algorithms.

With a monolithic structure, in fact, as soon as the simulation starts, the user loses ownership of the data and cannot access them interactively. This methodology has several drawbacks since it limits the user's capability to interact with the simulation because each interaction must be foreseen and implemented in the back end by modifying its source code and before starting the calculation. The monolithic approach runs on a sort of "autopilot" mode.

Another configuration would imply that the data objects devoted to calculation, while constructed via dedicated routines in the back end, belong to the upper software layer (front end). The front end is the owner of the data that are transferred through the interface to the back end, built as a library of pure functions that return the results after the required operations. According to this architecture, users may have access to the data on demand, and safely employ functionalities in the back end without the risk of side effects.

The NEMESI prototype developed within the CAMIVVER project (see Fig. 1) aims to let APOLLO3 move a step forward in supporting the library-based paradigm starting from well-defined user study objects. The front end allows for the definition of a case study thanks to dedicated Python modules, while the back end performs the calculation following a predefined sequence, acting as a wrapper of basic functionalities. At the end of the simulation, a multiparameter library object (MPO) is created to store the quantities of interest. The MPOs are suitable for APOLLO3 core calculations and may also be used for extracting information at the lattice level for verification and validation activities.

The front end consists of building blocks necessary to set up the simulation:

1. A repository with prebuilt, unstructured native (in APOLLO3 format) and nonnative (built using ALAMOS[7]) two-dimensional (2-D) geometries of the assemblies described in deliverable 4.3.[8]

2. A repository of calculation recipes in the form of user data files (UDFs) that contains predefined calculation blocks (i.e., JEFF3.1.1 nuclear data,[9] self-shielding options, etc.).

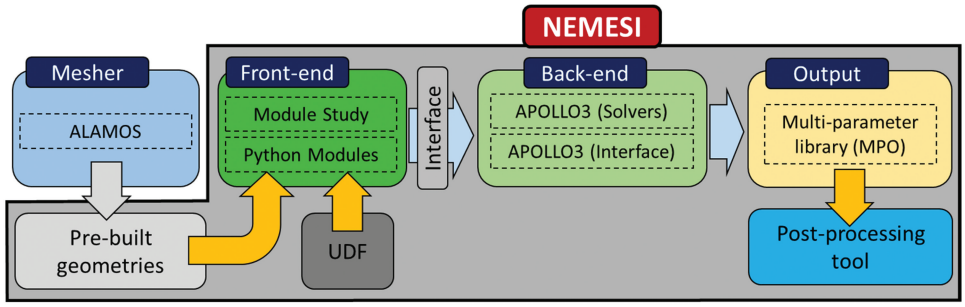

Fig. 1. Schematic representation of NEMESI.

3. Custom Python modules that wrap the APOLLO3 Python interface and add functionalities for manipulating back-end objects. Considering the present APOLLO3 architecture, this approach mimics the typical data exchange as if the back end was constructed as a library of functions so that further back-end improvements may be decoupled from the workflow in the front end.

The APOLLO3 internal interface and solvers constitute the back end. They represent the calculation kernel of NEMESI, which provides several solvers for the flux transport equation and numerical methods for self-shielding resonant isotopes, and includes methodologies to perform multilevel calculations.

The front end of NEMESI consists of multiple blocks (or classes) (see Fig. 2) that communicate with the back end, APOLLO3. When producing a MPO, first the user defines an object *Study* (right-pointing solid line in Fig. 3), which acts as the controller of the simulation, by indicating the parameters of the simulation, e.g., the assembly, the rod configurations, the burnup steps, the operating points, the flux normalization value, the type of output to be generated (i.e., *Mpo* and/or *Archive*, with the latter used for restart calculations), the homogenization mesh and energy, etc. If the initialization is successful, *Study* returns a success signal (left pointing dashed line) to the user and the operations can continue. The class *Study* uses the static class *Utils* to load the UDF predefined calculation recipes following the user input (see Fig. 3).

Then, with methods provided by *Study*, the user defines a *DepletionIterator* object to simulate the depletion of a chosen configuration (e.g., AllRodsOut). At the end of each burnup step calculation, the flux is normalized using the *FluxNorm* object, and the homogenized cross sections and isotope concentrations are eventually stored in separate dedicated HDF5 files, i.e., a MPO and an Archive, respectively (see Figs. 4 and 5), if the corresponding options are activated, i.e., the process executes the *opt* blocks. Later, branch calculations are distributed among multiple computational nodes, with each node/simulation computing the results for a rod configuration and a subset of the branch calculation points.

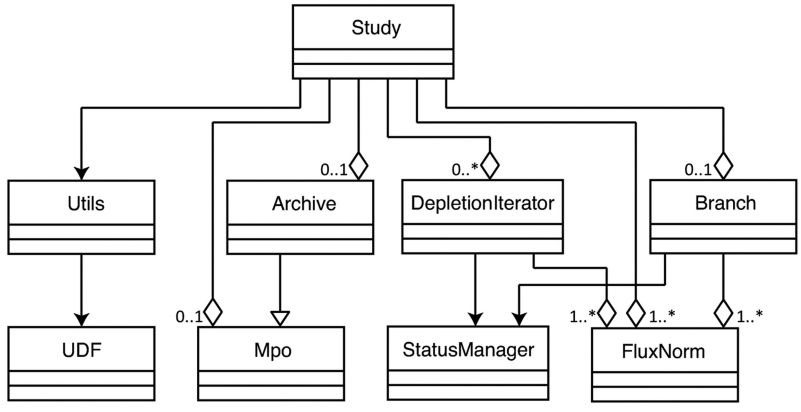

Fig. 2. Unified Modeling Language diagram for NEMESI front end (the arrow means is associated with and the diamond connection is aggregation, i.e., it composes a specific class).

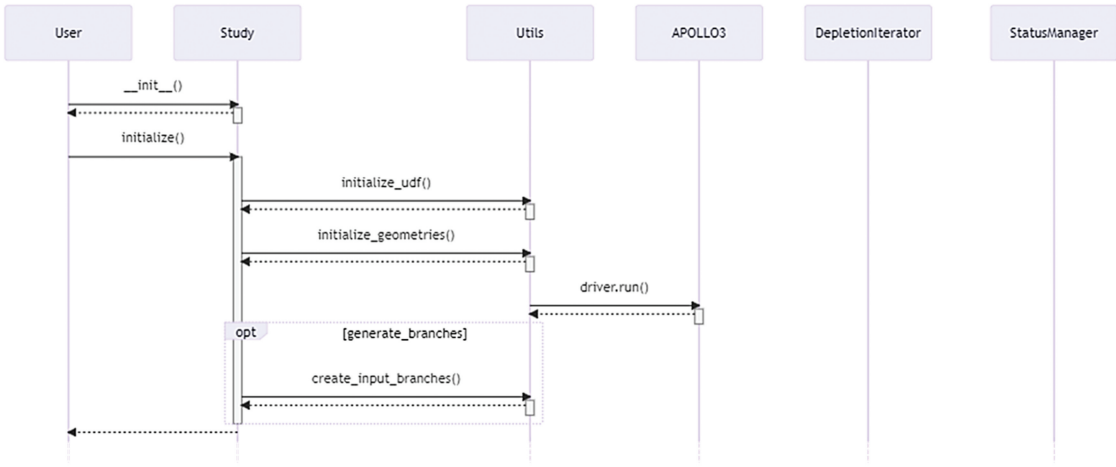

Fig. 3. Sequence diagram for NEMESI initialization. The solid line represents the send instruction and the returning dotted line represents the response of correct execution of the class.

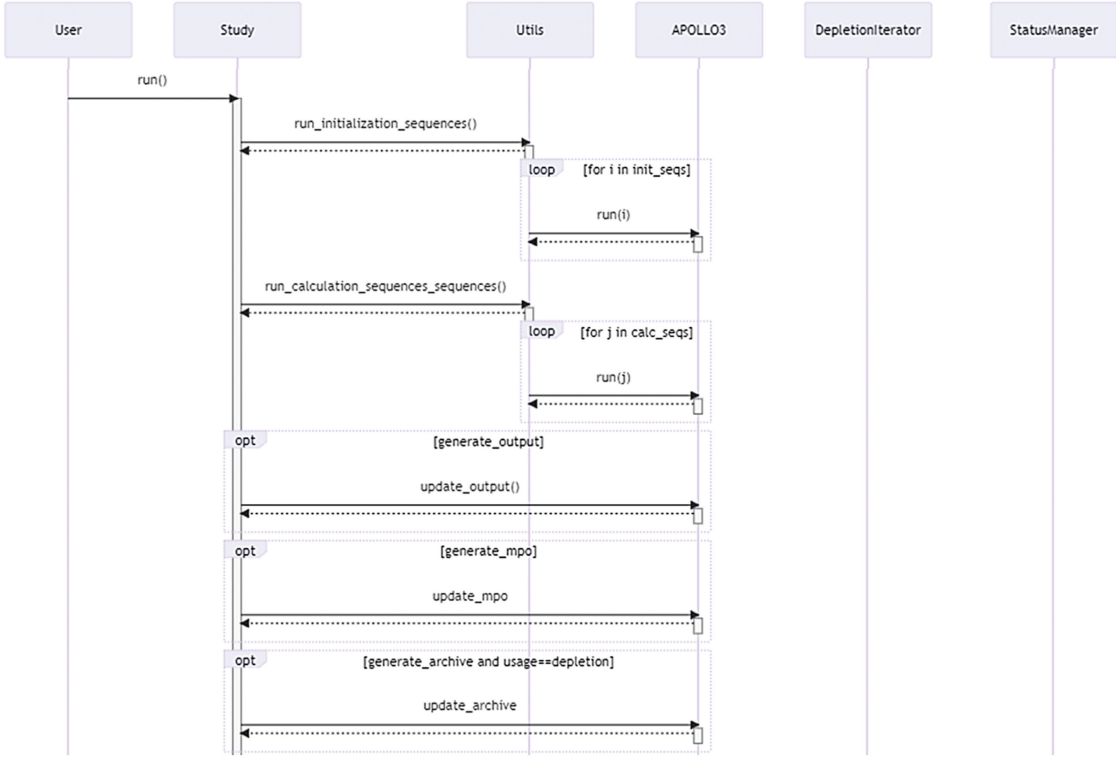

Fig. 4. Sequence diagram for NEMESI calculation of a single point. The solid line represents the send instruction and the returning dotted line represents the response of correct execution of the class.

Each simulation reinstantiates a *Study* object that, with the class *Archive*, reads the isotopic concentration at a specified burnup from the Archive HDF5 file. Then, with the object *Branch, Study* controls the calculations on the assigned operating points by changing the status of the computational kernel using the *StatusManager* static class (see Fig. 6) looping (block *loop*) on all the calculation points assigned to the *Branch*. Each simulation/

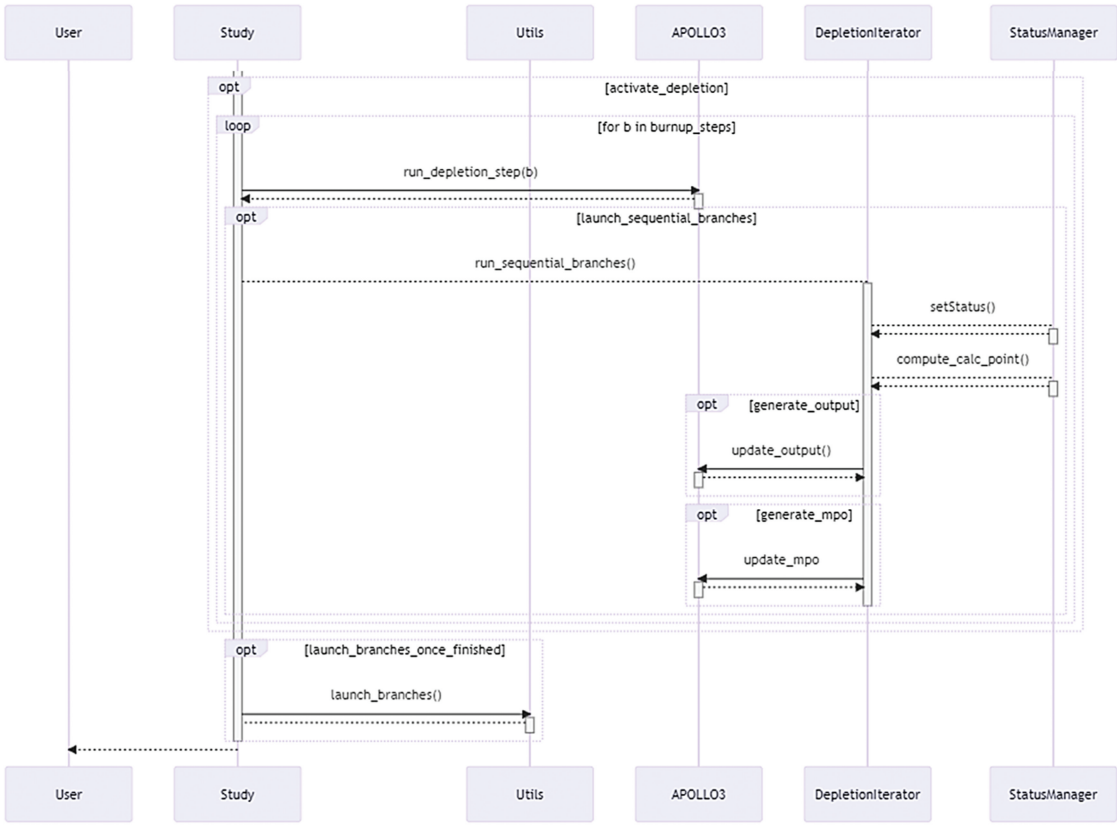

Fig. 5. Sequence diagram for NEMESI depletion calculation. Note that the branch calculation can be run sequentially after each depletion step or in parallel on multiple computational nodes once the evolution calculation is finished. The solid line represents the send instruction and the returning dotted line represents the response of correct execution of the class.

branch stores the homogenized cross sections for each operating point in its own MPO file.

Finally, the front end concatenates all these MPO files into a single file before their analysis or use in the core code. Despite the interactivity provided by the methods provided by the *Study* object, the user can also script the sequence of operations. The Python interpreter lately is able to execute this sequence of operations.

Only one prerequisite is necessary to run NEMESI: the *iapws*[10] Python module for computing water properties. The entire Python implementation respects the PEP8 guideline. The sequence diagram of NEMESI is represented in Figs. 3 through 6.

As test cases, the calculation platform has been used to compare the infinite medium multiplication eigenvalue (k_{inf}) at the beginning of life (BOL) of the selected assemblies, computed using the reference calculation scheme based on the SHEM-MOC scheme for PWRs[11] against available results of TRIPOLI-4®[12] and SERPENT2[13] simulations. The assemblies considered were those used for the validation activities of the CAMIVVER, and they included some of the Khmelnytskyï-2 and Kozloduy-6 VVER reactor fuel assemblies, an assembly for the 32-assembly small PWR core configuration,[14,15] and some assemblies from the KAIST benchmark.[16] The details about the assembly configurations, geometrical dimensions, material isotopic compositions, and operating conditions can be found in Ref. [8]. The comparison of computed k_{inf} values is shown in Table I.

The agreement between NEMESI and Monte Carlo codes observed for all VVER and PWR assemblies was very reasonable. Further investigations are foreseen in future work. The small discrepancies (a few pcm) between TRIPOLI-4 and SERPENT2 were presumed to come from one or a combination of these elements: different nuclear data processing systems (GALILEE versus NJOY) and nuclear data interpolation in temperature for the TRIPOLI-4 calculation. Since the present paper focuses mainly on VVER assembly calculations, only the depletion calculations for the 390GO and 30AV5 assemblies of the Khmelnytskyï reactor are compared to

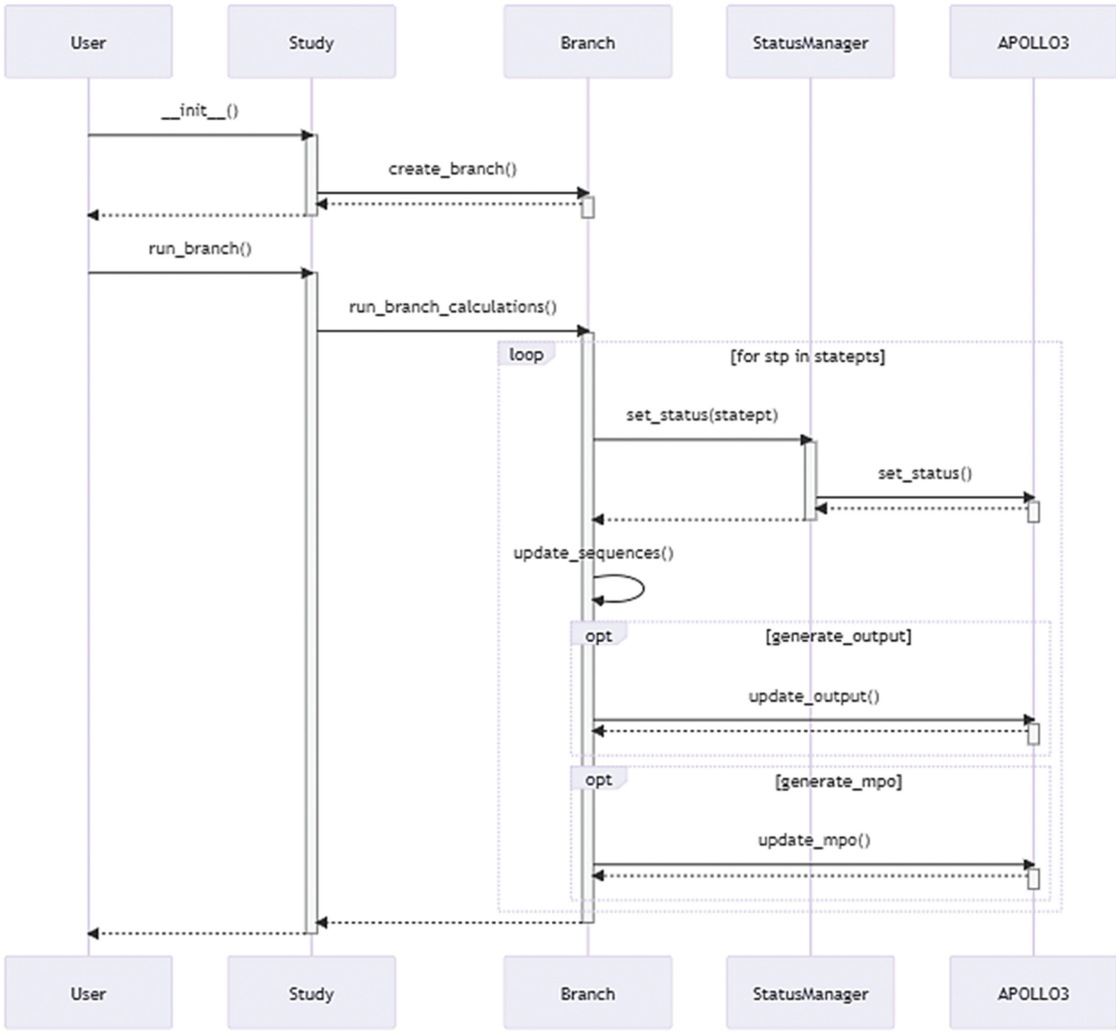

Fig. 6. Sequence diagram for NEMESI branch calculations when distributed in parallel on multiple computational nodes. The solid line represents the send instruction and the returning dotted line represents the response of correct execution of the class.

reference calculations. Still, the depletion calculation performed on the PWR assembly from Ref. [14], which is not shown here, gave a similar agreement.

Concerning the present analysis, assembly 390GO mainly consists of fuel pins with a 4.0% enrichment, and only the fuel pins on its boundary have a ^{235}U enrichment of 3.6%. The 390GO assembly includes some pins with a burnable absorber made of 3.3% ^{235}U and 5.0% gadolinium (Gd). Instead, assembly 30AV5 mainly consists of 3.0% ^{235}U-enriched pins and some pins with a 2.4% ^{235}U enrichment and 5.0% Gd. Both assemblies have stiffener plates in each corner to improve mechanical stability (see Fig. 7). The depletion simulations were performed considering an infinite media and the all-rods-out (ARO) configuration. The 2-D simulations were performed using the JEFF3.1.1 nuclear data library and a direct computational scheme using rotational boundary conditions to take advantage of the assembly symmetries.

Considering the burnup range from 0 to 60 GWd/t, the infinite multiplication factors have been compared to those obtained with SERPENT2 (see Fig. 8). This comparison showed that the root-mean-square error (RMSE) was about 60 pcm from 0 to ~8 GWd/t. This behavior may be slightly related to the different number of spatial rings discretizing the Gd pins used in the two codes, but more significantly to the nuclear data libraries and how they have been generated. Later, in the range from 8 to 30 GWd/t, the computed results get much closer to the reference Monte Carlo results with

TABLE I

Comparison of k_{inf} at BOL for the Selected Assembly Types[8]

Assembly (ARO)	TRIPOLI-4 (EDF)[a]	S2 (KIT)[b]	NEMESI (Framatome)		
	k_{inf}	k_{inf}	k_{inf}	$\Delta\rho_{T\text{-}4}$ (pcm)	$\Delta\rho_{S2}$ (pcm)
Khmelnytskyï-2 (VVER)					
13AU	0.96943 ± 5	0.96951 ± 3	0.96872	−75 ± 5	84 ± 3
30AV5	1.13966 ± 5	1.13929 ± 4	1.13810	−120 ± 5	−91 ± 4
390GO	1.24895 ± 5	1.24907 ± 4	1.24749	−94 ± 5	101 ± 4
FA3.3G	1.24164 ± 5	1.24160 ± 4	1.24060	96 ± 5	65 ± 4
KAIST (PWR)					
UOX at 2.0% enrichment	1.10444 ± 5	1.10443 ± 3	1.10486	34 ± 5	33 ± 3
UOX with Gd pins	1.04750 ± 5	1.04722 ± 4	1.04796	42 ± 5	67 ± 4
Mixed oxide	1.16349 ± 5	1.16350 ± 4	1.16483	98 ± 3	98 ± 4
32-Assembly Small Core (PWR)					
UOX at 3.7% enrichment	1.30554 ± 5	1.30456 ± 4	1.30568	−8 ± 3	68 ± 4

[a]Reactivity difference with respect to TRIPOLI-4 calculations.
[b]Reactivity difference with respect to SERPENT2 calculations.

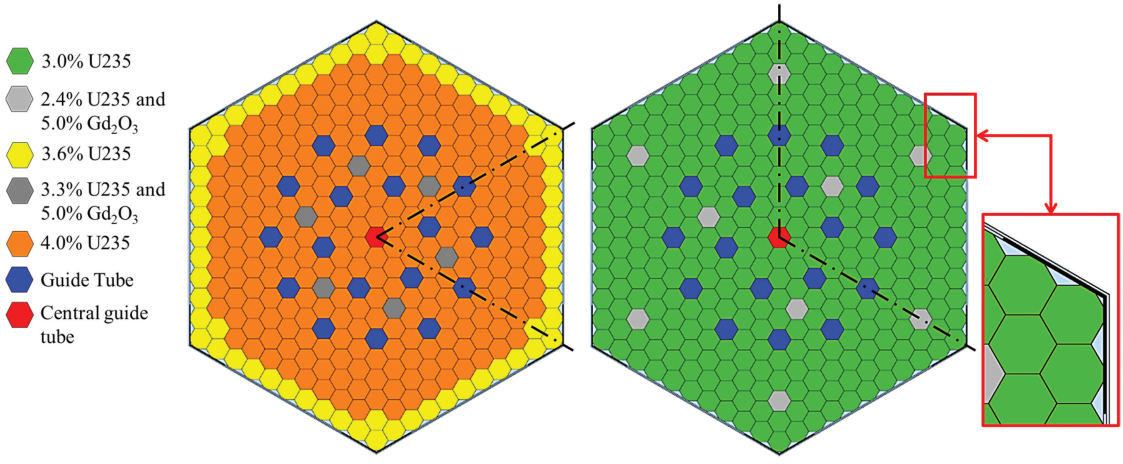

Fig. 7. (left) 390GO and (right) 30AV5 assembly configurations.[8] The inset shows the stiffener plate. The applicable symmetry is indicated with black dash-dotted lines.

a RMSE of about 11 pcm and 58 pcm for the 390GO and 30AV5 assemblies, respectively, showing a good agreement of the two calculations with the respective reference results. Finally, after 30 GWd/t, the curves start to diverge, probably because of the different formulas used to compute the released energy[17] in APOLLO3 and SERPENT2,[18] with a RMSE of about 170 pcm and 310 pcm for the 390GO and 30AV5 assemblies, respectively.

Despite the highlighted differences, the preliminary results are encouraging; however, SERPENT2 cannot be considered a reference yet because of the

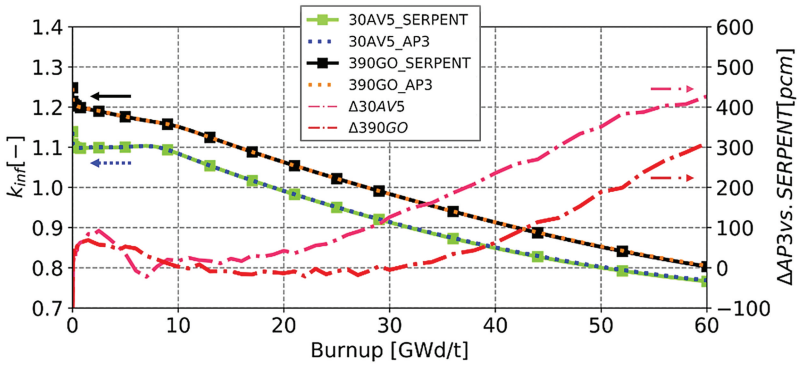

Fig. 8. 390GO and 30AV5: Comparison of NEMESI and SERPENT k_{inf} (left axis) and their difference (right axis) during depletion calculation.

different energy deposition model, as it does not account the energy emitted by gammas. New modified evaluated nuclear data libraries are being developed that should eliminate the discrepancies between the two codes, as the power produced will be computed in the same way.

III. VVER CALCULATION SCHEME AND DISCUSSION

III.A. Self-Shielding Grouping

The state-of-the-art computational schemes available for industrial applications in French deterministic codes are SHEM-MOC[11] and REL2005.[19] The second is derived from the former, and both are explicitly tailored for PWRs.

Nevertheless, these schemes cannot be straightforwardly applied to the VVER cases due to the present limitations of the back end. This is because the solver is based on the interface–current collision probability method (IC-CPM), which is not yet fully compatible with the unstructured geometries produced by ALAMOS. Therefore, the current work also presents some preliminary results for developing a computational scheme suitable for VVER assemblies that is aimed at reducing the calculation time without reducing the accuracy of the results. The proposed options described here were derived from CEA's activity performed in the CAMIVVER project.

Looking in more detail at the reference scheme, the two-three Dimensional Transport collision probability method (TDT-CPM) self-shielding problem considers each self-shielded region as a separate self-shielding

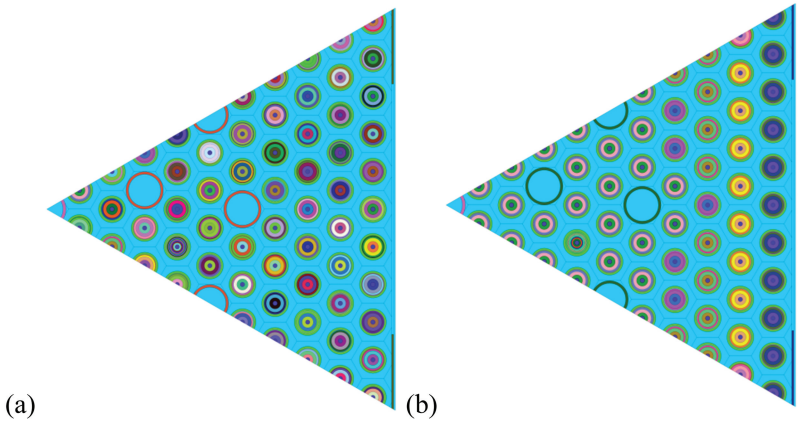

Fig. 9. (a) REFERENCE and (b) INDUSTRIAL self-shielding grouping for assembly 390GO. Each color corresponds to a different property/medium in the self-shielding calculations.

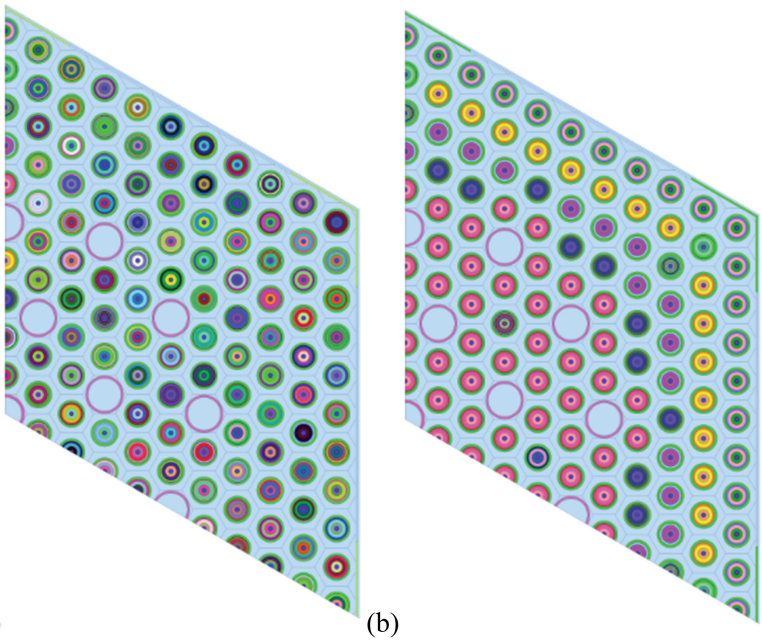

(a) (b)

Fig. 10. (a) REFERENCE and (b) INDUSTRIAL self-shielding grouping for assembly 30AV5. Each color corresponds to a different property/medium in the self-shielding calculations.

medium (see Figs. 9a and 10a). This means that mixture probability tables and the corresponding self-shielded cross sections must be computed for all the n regions of the computational geometry.

In the back end under test, the first feature implemented to reduce the calculation time was the so-called self-shielding grouping; the regions were grouped in m different self-shielding media. A group may include various pins with the same material or with a similar position in the assembly lattice (e.g., close to a guide tube, a control rod, Gd fuel pins, or the corners of the assembly, etc.) (see Figs. 9b and 10b), which allows the self-shielding solver to consider only $m < n$ computational zones (or groups).

In NEMESI, by changing the calculation scheme parameter of the *Study* class, the user can choose between two different calculation schemes: REFERENCE (no self-shielding grouping) and INDUSTRIAL (with self-shielding grouping). Please note that the choice of the word INDUSTRIAL is arbitrary, and it has nothing to do with actual industrial applications.

The results in Table II show that with the INDUSTRIAL scheme, the computational cost for the solution of the self-shielding problem is from two to three times smaller than that for the REFERENCE scheme, without reducing the accuracy of the obtained k_{inf} values and the flux distribution (see Figs. 11 and 12) for which absolute relative error on the pin-by-pin distribution is always smaller than 3×10^{-5} and 8×10^{-5} (close to the flux convergence criteria of 10^{-5}) for the 390GO and the 30AV5, respectively, proving the coherence of the two calculation schemes.

The observed reduction of computational time becomes a significant advantage when performing depletion calculations during which the self-shielding problem is solved multiple times. Looking at the depletion calculation for these two considered assemblies (see Fig. 13), one can notice that the difference in the k_{inf} computed with the two computational schemes reaches its maximum of ~7 pcm (in absolute value) when the burnup is ~40 GWd/t, probably due to slightly different isotopic composition evolution. However, with respect to the REFERENCE scheme, the INDUSTRIAL one is conservative in computing the reactivity, and depending on the assembly, the total computational time for the same 70-burnup-point structure is reduced by a factor ranging from ~2.6 to ~5.3 and is always smaller than the one required by SERPENT2. With such results, one may conclude that even if the INDUSTRIAL calculation scheme may not satisfy all the industrial requirements in terms of performance, this can be considered a good starting point for further developing the calculation scheme and demonstrating the platform's capabilities.

TABLE II

390GO and 30AV5: k_{inf} and Calculation Time Comparisons

Parameter	390GO		30AV5	
Calculation scheme	REFERENCE	INDUSTRIAL	REFERENCE	INDUSTRIAL
Symmetry Number or regions	1/6 5496		1/3 10 935	
k_{inf} at BOL	1.24742	1.24742	1.13810	1.13810
Self-shielding solver	TDT-CPM			
Self-shielding grouping Time for self-shielding calculation	No 2 h 18 min	Yes (9 groups) 57 min	No 9 h 29 min	Yes, (11 groups) 3 h
Flux solver	TDT-MOC			
Time for flux calculaton[a,b] Time for 70-burnup-point calculation	2 h 50 min 1335 h 51 min	3 h 10 min 513 h 57 min	5 h 25 min 5570 h 2 min	5 h 29 min 1054 h 26 min

[a]NEMESI simulations run on Intel® Xeon® Platinum 8260 CPU @ 2.40-GHz cores with 48 OpenMP threads.
[b]SERPENT2 calculations run on Intel® Xeon® Platinum 8368 CPU @ 2.40-GHz cores with 150 OpenMP threads. The simulation on the full assembly geometry lasted about 59 h, and the 70-burnup-point simulation lasted 2165 h.

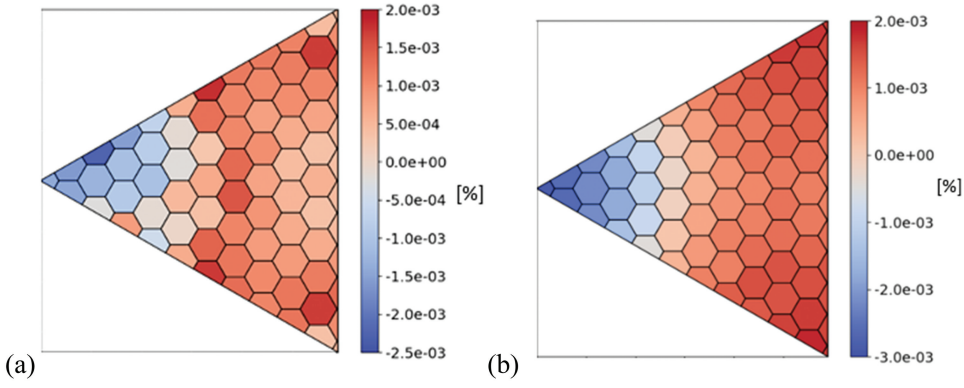

Fig. 11. 2-D distributions of (a) fast and (b) thermal flux relative error for the 390GO assembly with the REFERENCE and the INDUSTRIAL calculation schemes.

Again, the flux distribution alone is not enough to guarantee the accuracy of the solution when the self-shielding grouping is used. Therefore, here the comparison of the fast absorption and thermal fission rates for ^{235}U are presented in Figs. 14 and 15, which show that implementation of the proposed self-shielding grouping does not deteriorate the quality of the computed reaction rates. It remains true, according to the presented explanation, that the self-shielding grouping is chosen according to geometric considerations, which in a certain way can reflect the physical phenomena. In more heterogeneous configurations, or when large flux gradients are expected, the self-shielding grouping is a more delicate choice, as it can diverge from the actual physics.

Again, looking at the population of the selected isotopes, namely, ^{235}U, ^{238}U, ^{239}Pu, and ^{241}Am and ^{155}Gd, ^{156}Gd, ^{157}Gd, and ^{158}Gd, for assembly 390GO (see Figs. 16 and 17) and assembly 30AV5 (see Figs. 18 and 19), respectively, the two presented

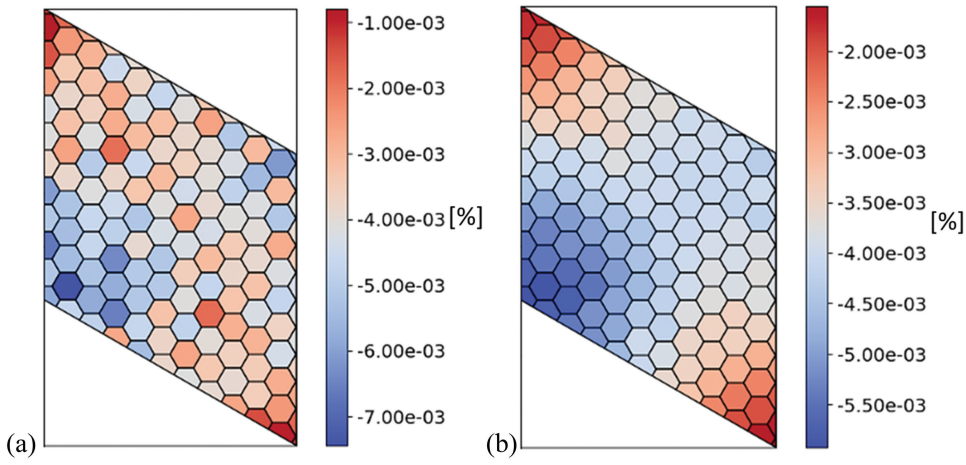

Fig. 12. 2-D distributions of (a) fast and (b) thermal flux relative error for the 30AV5 assembly with the REFERENCE and the INDUSTRIAL calculation schemes.

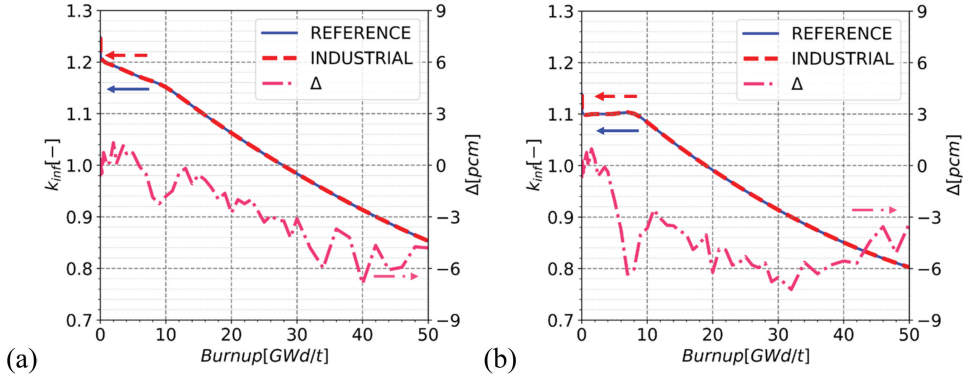

Fig. 13. k_{inf} during depletion calculation with REFERENCE and INDUSTRIAL schemes: (a) 390GO and (b) 30AV5. The difference between the two curves is shown on the right axis.

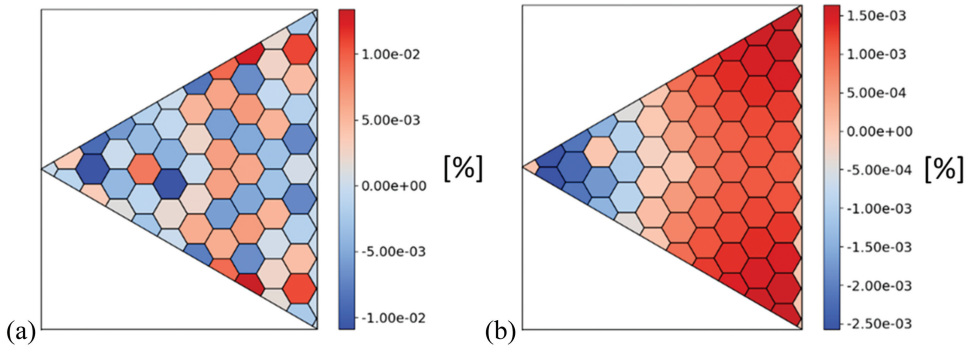

Fig. 14. Relative error between the INDUSTRIAL and SHEMMOC calculation schemes of the (a) fast absorption and (b) thermal fission reaction rates for the 390GO assembly.

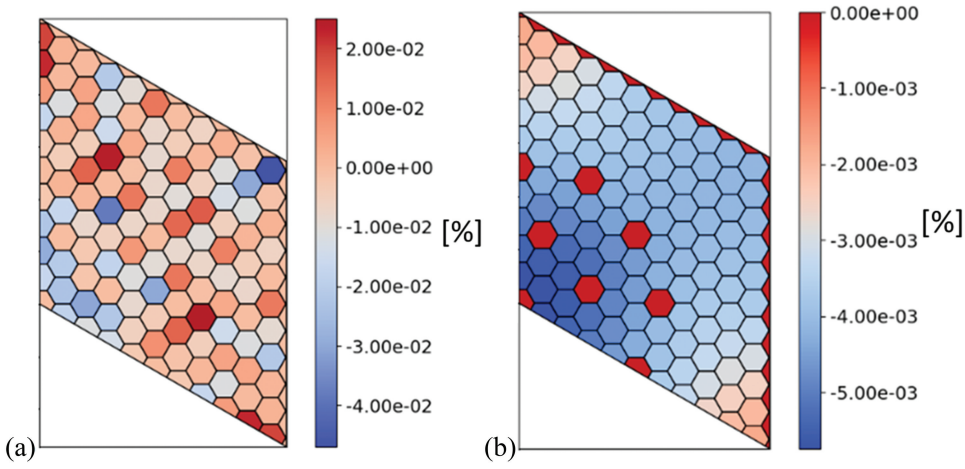

Fig. 15. Relative error between the INDUSTRIAL and SHEMMOC calculation schemes of the (a) fast absorption and (b) thermal fission reaction rates for the 30AV5 assembly.

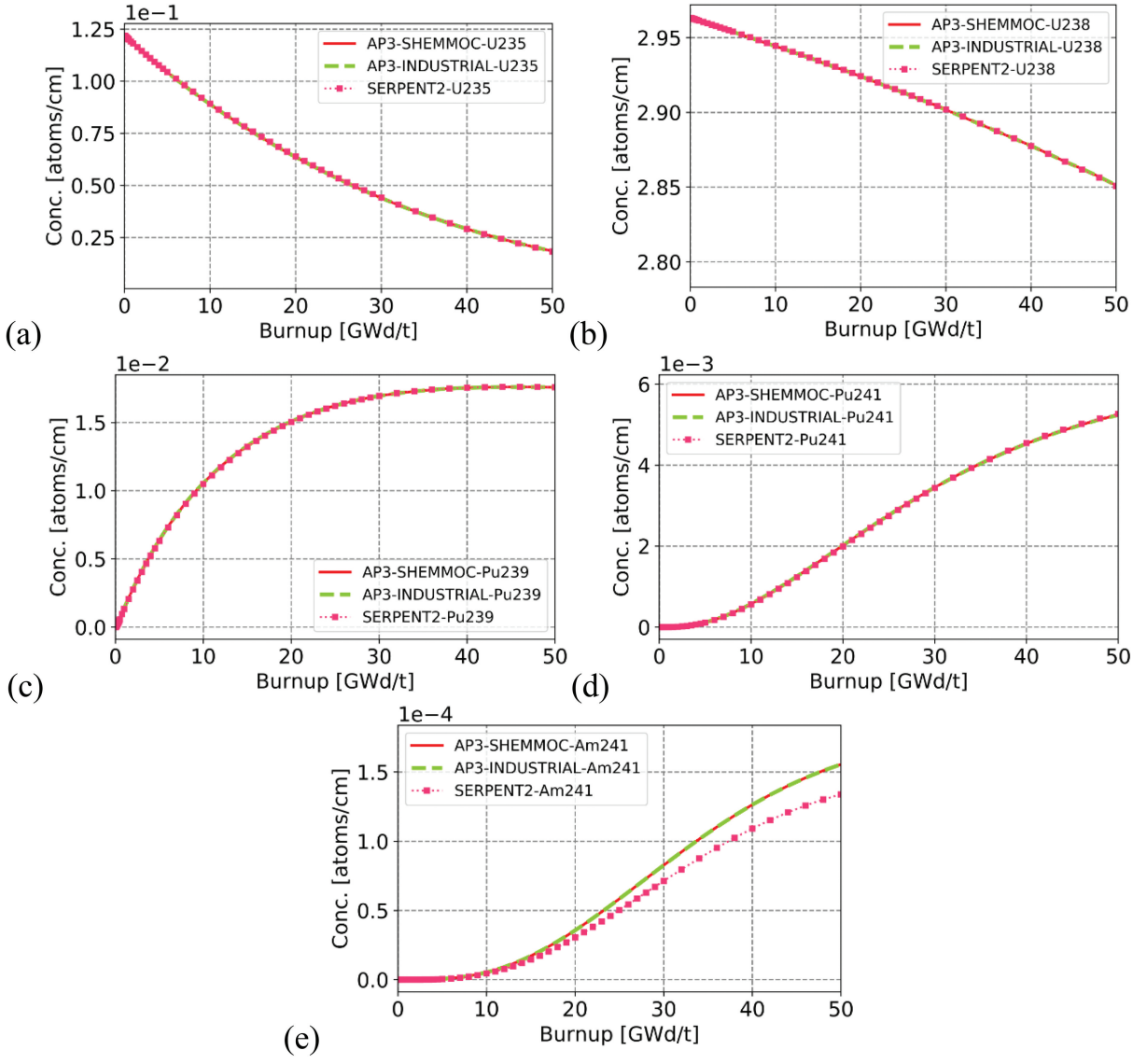

Fig. 16. Evolution of selected U, Pu, and Am isotopic linear atomic densities for assembly 390GO.

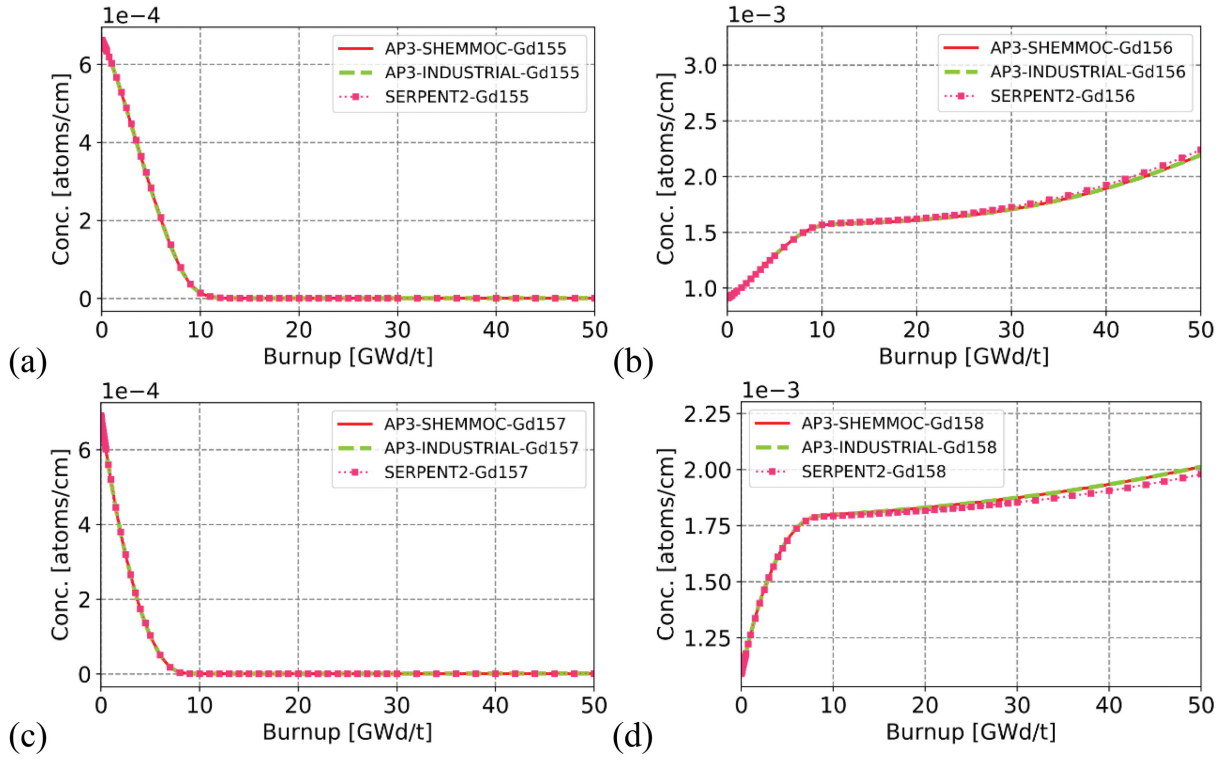

Fig. 17. Evolution of Gd isotopic linear atom densities for assembly 390GO.

calculation schemes show in general good results. The volumetric concentrations have been integrated into the region volumes because in APOLLO3 the homogenized output surface corresponds to the whole, while in SERPENT2 it considers only the fuel pins.

Since in the present comparisons the focus is only on fissile and burnable poison isotopes, by integrating the volumetric concentrations into the respective homogenized surfaces, a linear concentration (per axial length unit) can be obtained. The results shows that at low burnup during Gd consumption, during which sensitive k_{inf} differences have been observed, the relative error on the concentrations of Pu, Am, and Gd, computed with point-by-point comparisons of the results provided by the two codes, can be very large (see Figs. 20 and 21) due to the multiple effects mentioned previously, i.e., spatial discretization of Gd pins and different depletion chains. After 10 GWd/t, the relative errors stabilize around a few percent. The error on the ^{235}U concentration is very good and starts increasing at high burnups, where small differences in small absolute concentrations can result in large relative errors. The error on the ^{238}U concentrations is excellent all along the evolution, as shown in Fig. 20.

The drift of the ^{241}Pu and ^{241}Am isotope populations at high burnup is probably related to the different modeling and simplifications of the depletion chains used in the two codes and a different modeling of the depletion or the use of the already mentioned differences in the nuclear data libraries used. The same reason may also explain the slight drift in the ^{156}Gd and ^{158}Gd populations. The CAMIVVER project focused on the development of an industrial prototype. To support this development, several verification activities were carried out as presented in this paper. The validation strategy is under definition and several experimental data will be considered. A follow-up project is proposed to support further development and validation.

III.B. Other Possible Calculation Scheme Evolutions

The parametric studies performed here represent only the first step toward the definition of an industrial computational scheme for VVER reactors. Additional actions can be taken to optimize the

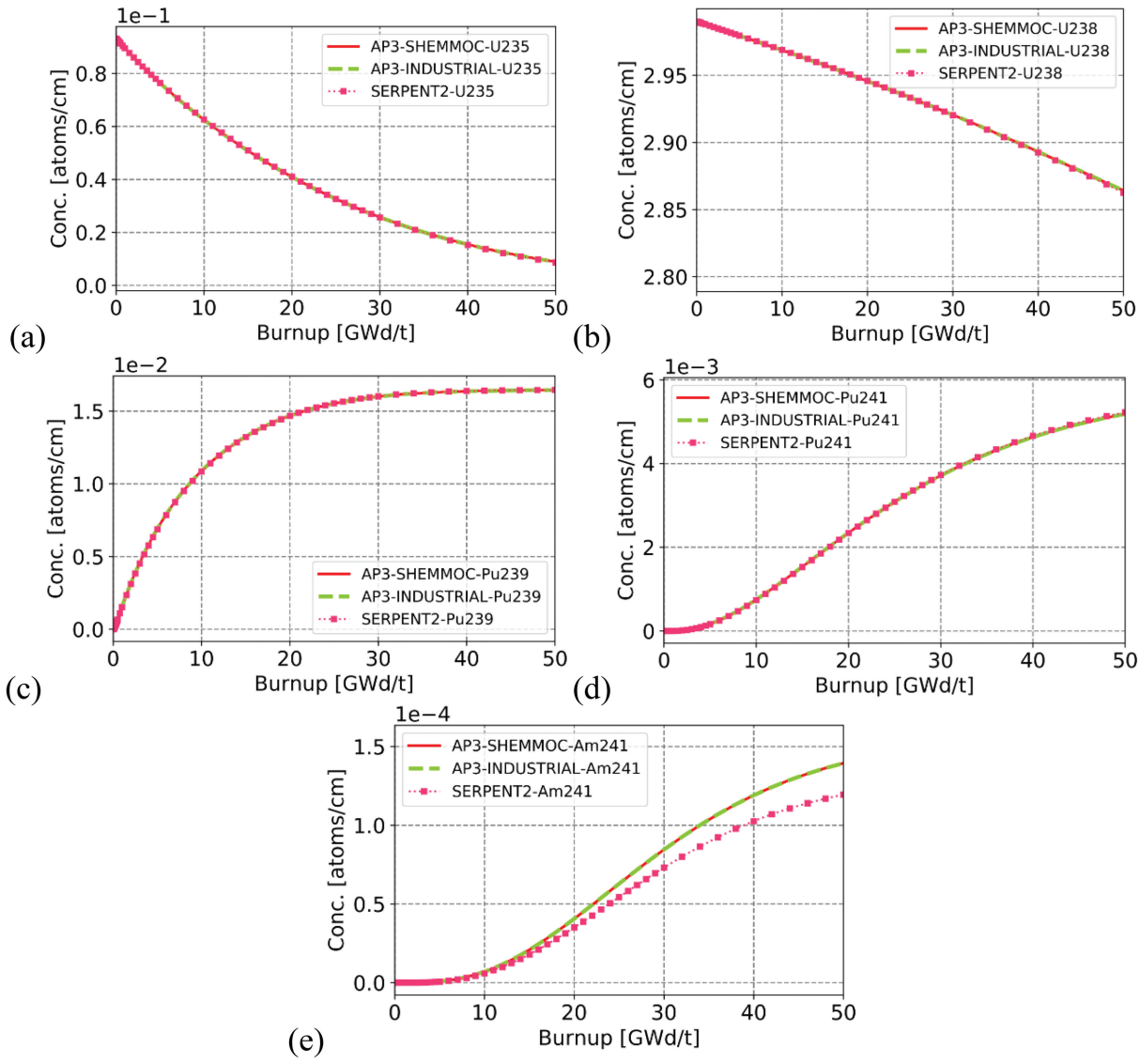

Fig. 18. Evolution of selected U, Pu, and Am isotopic linear atom densities for assembly 30AV5.

computational scheme, including, for instance, a sensitivity analysis on the geometrical mesh refinement for the pins, an optimization of the computational sequences (e.g., performing self-shielding calculation only at selected burnup points), a reduction in the number of points of the depletion mesh, or again implementing a multilevel computational scheme inspired from REL2005.[19]

IV. CONCLUSIONS

The variety of users and application cases of computational tools in nuclear research and industry justify the specification of different software requirements to be satisfied. Following preliminary work that aims to define a systematic requirement-based approach to build a neutronics study platform, this work presented NEMESI, the multiparameter library generator prototype developed in the framework of the EU H2020 CAMIVVER.

NEMESI aims to implement a modern library-based software architecture, dividing the platform's responsibilities into its different components: the front end for interaction with the users, and the back end based on APOLLO3, constituting the computational kernel, communicating via an interface that defines the exchange of

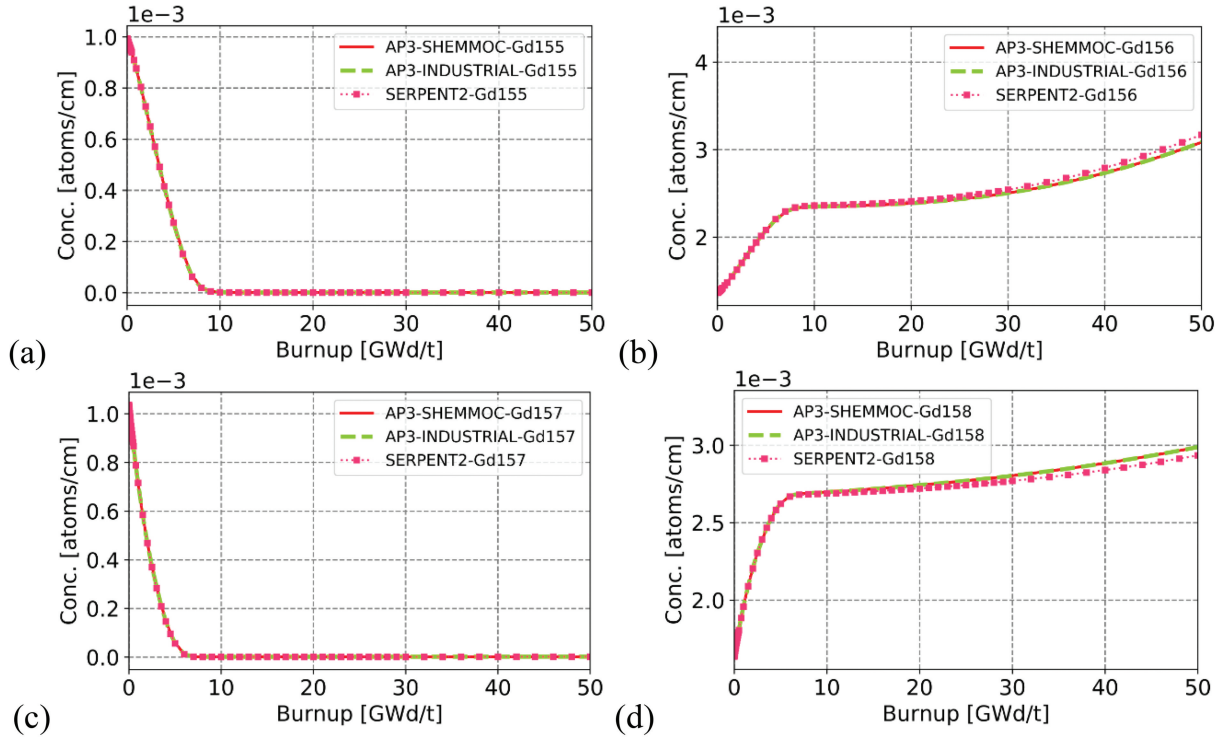

Fig. 19. Evolution of Gd isotopic linear atom densities for assembly 30AV5.

the data objects and the relevant function calls to perform the calculations.

After describing NEMESI's rationale and structure, some simulation comparisons were shown to assess the tool's accuracy. The computed infinite multiplication factors for VVER and PWR assemblies were compared to those obtained using TRIPOLI-4 and SERPENT2, indicating a good agreement with a RMSE of about 110 pcm and 172 pcm for the 390GO and the 30AV5 assemblies, respectively.

The assessment of the accuracy and precision of the calculation platform continued by comparing NEMESI/APOLLO3 depletion calculations for two VVER assemblies, i.e., the Khmelnytskyï 30AV5 and 390GO, with SERPENT2 showing that the computed results were in good agreement up to 8 GWd/t during the Gd burn, with a difference up to 100 pcm, and then in good agreement from 8 to 30 GWd/t with stable differences up to 10 and 40 pcm, respectively, for the two assemblies. In the last portion of the simulated depletion, the differences started to increase, possibly because of the different power formulas used in the two codes.

When comparing selected isotope populations, the NEMESI-APOLLO3 computed results were in good agreement with those obtained with SERPENT2; the relative error was a few percent at low burnup values, but tended to increase as the burnup increased. The reason behind the increase in relative errors could be the use of different depletion chains in APOLLO3 and SEPRENT2 (for Pu and Am isotopes) or the fact that the relative error was computed on small values (for Gd isotopes).

The last part of the present work dealt with a preliminary step in defining the VVER calculation scheme, which has yet to be fully validated and shown in the literature. The first feature proposed was self-shielding grouping, which treats the pins with the same self-shielded property, i.e., depending on the material and/or the pins in similar locations inside the assembly lattice. The simulations performed with the INDUSTRIAL computational scheme were in excellent agreement concerning the reference results on the k_{inf} ($\Delta < 7$ pcm) and the flux distribution ($\varepsilon_{err} < 0.2\%$) and showed a reduction in the computational time by a factor of 3.

Looking at the isotope concentrations during the depletion, the APOLLO3 results were in very good agreement with those computed by SERPENT2, with larger discrepancies during the Gd consumption that then were reabsorbed at higher burnups. The reason behind these increasing differences is probably related to the different geometrical discretization of Gd pins and the different depletion chains used in the two codes. To sum up, all these considerations assessed the successful development of NEMESI as a multiparameter generator and the precision of the numerical methods of APOLLO3 (the computational kernel) for validation exercises and defining a suitable computational scheme for VVER and PWR assemblies.

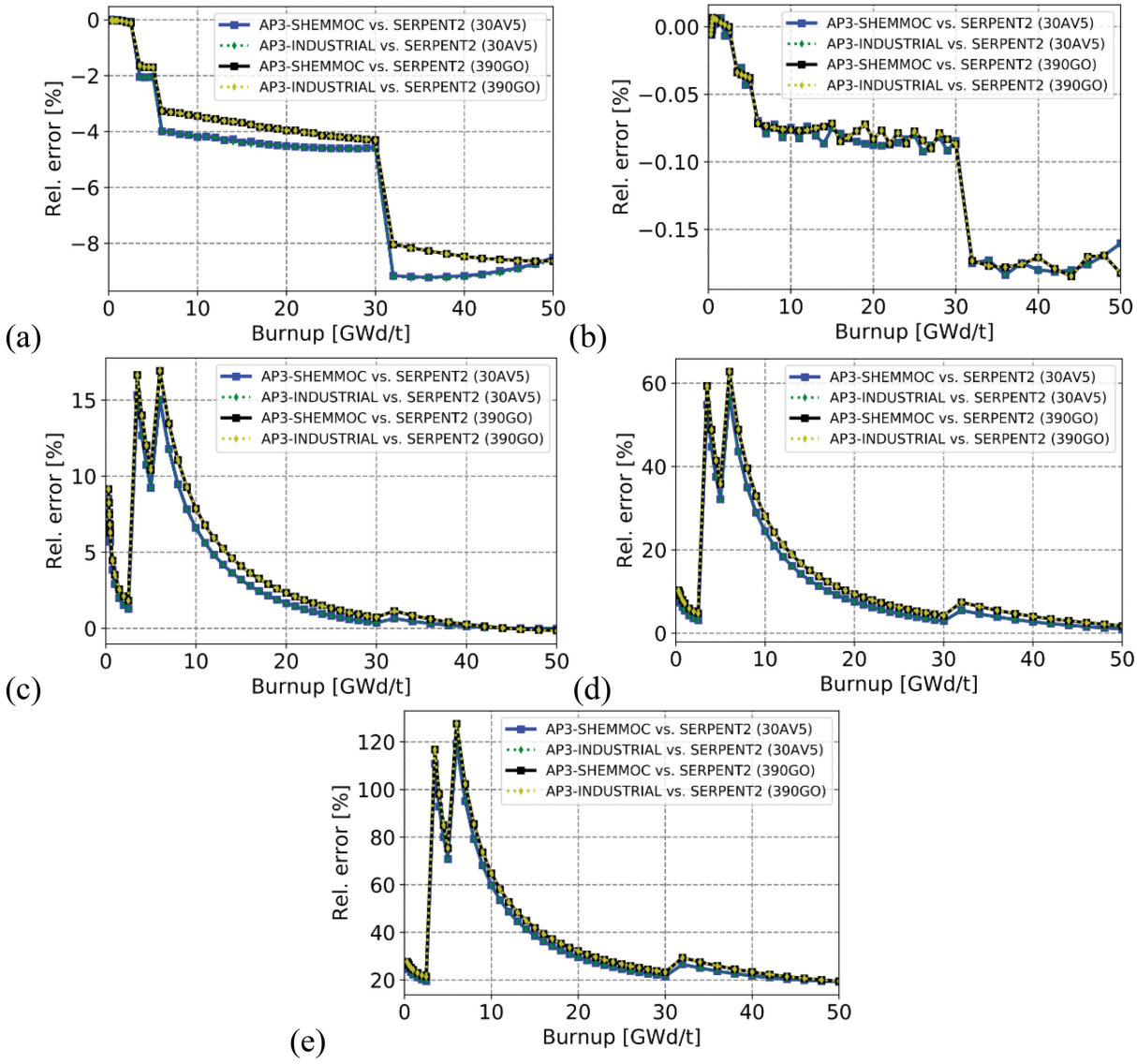

Fig. 20. Error on (a) ^{235}U, (b) ^{238}U, (c) ^{239}Pu, (d) ^{241}Pu, and (e) ^{241}Am linear atom densities for assemblies 30AV5 and 390GO with different calculation schemes.

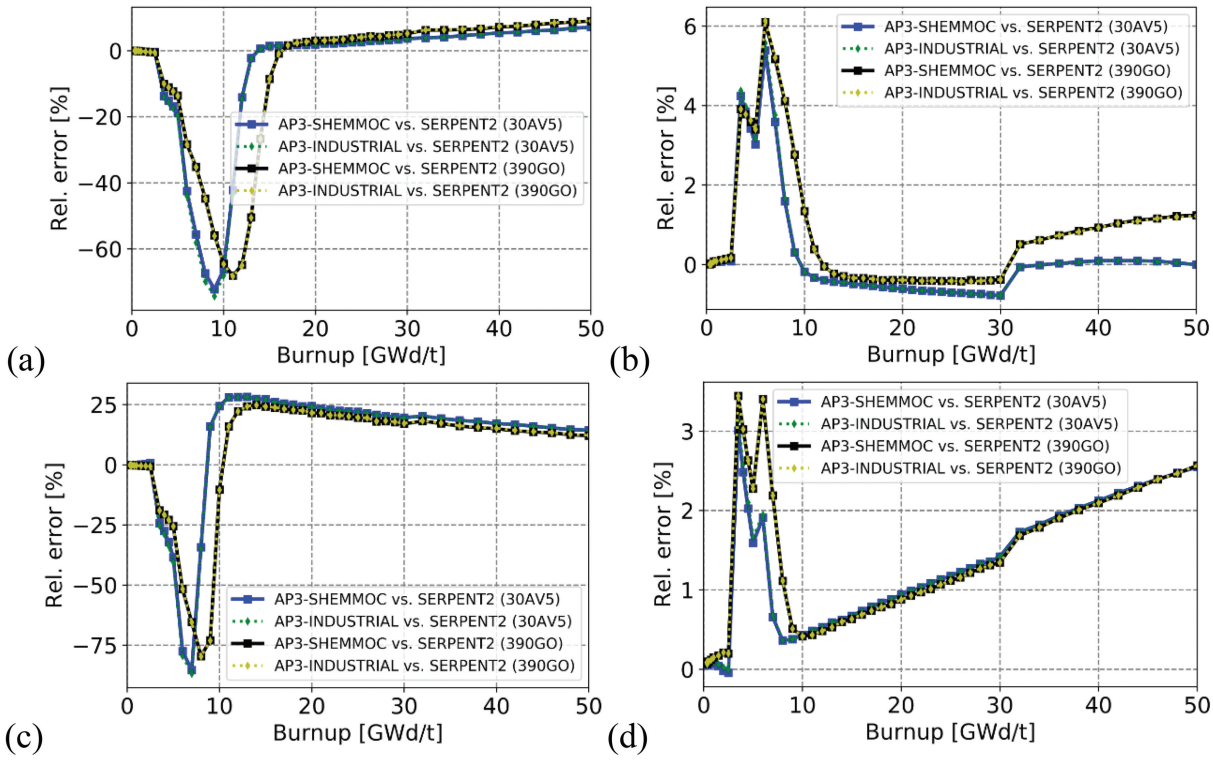

Fig. 21. Error on (a) ^{155}Gd, (b) ^{156}Gd, (c) ^{157}Gd, and (d) ^{158}Gd linear atom densities for assemblies 30AV5 and 390GO with different calculation schemes.

Acknowledgments

APOLLO3® is a registered trademark of CEA. The CAMIVVER project received funding from the Euratom Research and Training Programme 2019–2020 under grant agreement no. 945081.

Disclosure Statement

No potential conflict of interest was reported by the authors.

Funding

The CAMIVVER project received funding from the Euratom Research and Training Programme 2019-2020 under grant agreement No 945081.

ORCID

A. Brighenti http://orcid.org/0000-0003-4775-9375
B. Vezzoni http://orcid.org/0000-0003-3934-3505
A. Hebert http://orcid.org/0000-0002-2065-1041

References

1. D. VERRIER et al., "Codes and Methods Improvements for VVER Comprehensive Safety Assessment: The CAMIVVER H2020 Project," *Proc. Int. Conf. ICONE-28* (2021).
2. B. CALGARO and B. VEZZONI, "Advanced Couplings and Multiphysics Sensitivity Analysis Supporting the Operation and the Design of Existing and Innovative Reactors," *Energies*, **15**, *9*, 3341 (2022); https://doi.org/10.3390/en15093341.
3. L. MERCATALI et al., "Advanced Multiphysics Modeling for PWR and VVER Applications, Conference," *Proc. Int. Conf. ICAPP2023*, Gyeongju, Korea, April 23–27, 2023.
4. P. MOSCA et al., "APOLLO3®: Overview of the New Code Capabilities for Reactor Physics Analysis," *Proc. Int. Conf. M&C2023*, Niagara Falls, Ontario, Canada, August 13–17, 2023; https://cea.hal.science/cea-04469092.
5. A. PREVITI et al., "Towards a Systematic Requirement-Based Approach to Build a Neutronics Study Platform," *Nucl. Sci. Eng.* **197**, *9*, 2459 (2023); https://doi.org/10.1080/00295639.2023.2189535.

6. A. HEBERT, *Applied Reactor Physics*, p. 210, Presses Internationales Polythecnique, Montréal, Canada (2009).
7. D. TOMATIS et al., "Overview of SERMA's Graphical User Interfaces for Lattice Transport Calculations," *Energies*, **15**, *4*, 1417 (2022); https://doi.org/10.3390/en15041417.
8. A. WILLIEN and B. VEZZONI, "Definitions of the Tests Cases for the Verification Phases of the Multi-Parametric Library Generator," CAMIVVER; http://www.camivver-h2020.eu/src/assets/doc/D4-3.pdf (current as of Feb. 11, 2021).
9. A. SANTAMARINA et al., "The JEFF-3.1.1 Nuclear Data Library. Validation Results from JEF-2.2 to JEFF-3.1.1," *Nucl. Energy Agency* (2009).
10. International Association for the Properties of Water and Steam; http://www.iapws.org/ (current as of July 21, 2022).
11. A. SANTAMARINA et al., "Recent Advances in Accurate Neutronic Calculation of GEN-3 LWR Reactors," *Ann. Nucl. Energy*, **87**, *1*, 68 (2016); https://doi.org/10.1016/j.anucene.2015.05.035.
12. E. BRUN et al., "Tripoli-4®, CEA, EDF and AREVA Reference Monte Carlo Code," *Ann. Nucl. Energy*, **82**, 151 (2015); https://doi.org/10.1016/j.anucene.2014.07.053.
13. J. LEPPÄNEN et al., "The Serpent Monte Carlo Code: Status, Development and Applications in 2013," *Ann. Nucl. Energy*, **82**, 142 (2015); https://doi.org/10.1016/j.anucene.2014.08.024.
14. A. GODFREY, "VERA Core Physics Benchmark Progression Problem Specifications, Revision 4," CASL-U-2012-0131-004 (Aug. 29, 2014).
15. J. BLANCO and B. CALGARO, *D5.1—Description of the Core Reference Test Cases—Part 1*, CAMIVVER; http://www.camivver-h2020.eu/src/assets/doc/D5-1.pdf (current as of Aug. 31, 2021).
16. N. Z. CHO, "Benchmark Problem 1A: MOX Fuel-Loaded Small PWR Core (MOX Fuel with Zoning)," ; http://nurapt.kaist.ac.kr/benchmark.
17. A. BENNETT, N. MARTIN, and M. SCHNEIDER, "Validation of APOLLO2-A Against SERPENT2 on BWR Lattices," *Proc. Int. Conf. M&C2019*, Portland, Oregon (2019).
18. L. MERCATALI, N. BEYDOGAN, and V. SANCHEZ-ESPINOZA, "Simulation of Low-Enriched Uranium Burnup in Russian VVER-1000 Reactors with the Serpent Monte-Carlo Code," *Nucl. Eng. Technol.*, **53**, *9*, 2830 (2021); https://doi.org/10.1016/j.net.2021.03.
19. J. F. VIDAL et al., "New Modeling of LWR Assemblies Using the APOLLO2 Code Package," *Proc. Int. Conf. M&C2007*, Monterey, California, April 14–19, 2007.